ELSEVIER

Journal of Fluids and Structures 24 (2008) 111–128

JOURNAL OF FLUIDS AND STRUCTURES

www.elsevier.com/locate/jfs

Dynamics of a long tubular cantilever conveying fluid downwards, which then flows upwards around the cantilever as a confined annular flow

M.P. Païdoussis*, T.P. Luu, S. Prabhakar

Department of Mechanical Engineering, McGill University, 817 Sherbrooke Street West, Montreal, Qué., Canada H3A 2K6

Received 2 October 2006; accepted 11 July 2007
Available online 12 September 2007

Abstract

A theoretical model is developed for the dynamics of a hanging tubular cantilever conveying fluid downwards; the fluid, after exiting from the free end, is pushed upwards in the outer annular region contained by the cantilever and a rigid cylindrical channel. This configuration thus resembles that of a drill-string with a floating fluid-powered drill-bit. The linear equation of motion is solved by means of a hybrid Galerkin–Fourier method, as well as by a conventional Galerkin method. Calculations are conducted for a very slender system with parameters appropriate for a drill-string, for different degrees of confinement of the outer annular channel; and also for another, bench-top-size experiment. For wide annuli, the dynamics is dominated by the internal flow and, for low flow velocities, the flow increases the damping associated with the presence of the annular fluid. For narrow annuli, however, the annular flow is dominant, tending to destabilize the system, giving rise to flutter at remarkably low flow velocities. The mechanisms underlying the dynamics are also considered, in terms of energy transfer from the fluid to the cantilever and *vice versa*, as are possible applications of this work.

Keywords: Pipe conveying fluid; Cylinder in axial flow; Drill-string; Floating drill-bit; Oscillatory instabilities; Low critical flow velocities; MEMS applications

1. Introduction

An alternative title of this paper might have been "The dynamics of an idealized flow-powered drill-string with a floating drill-bit", since that system motivated this study. Fig. 1 shows the idealized system, consisting of a hollow drill-rod and a floating drill-bit, i.e. one that is not mechanically attached to the drill-rod. Sludge, pumped down within the hollow rod, rotates the drill-bit as a turbine, thus drilling into the rock. The sludge together with the debris flows upwards around the drill rod to the surface. This system was granted a fallacious patent, as charmingly related by Den Hartog (1969), by claiming that, as there would be no compressive force in the drill-string as in traditional drilling, this system would not buckle under normal operating conditions; in a traditional rotating drill-string a great deal of energy

*Corresponding author. Tel.: +1 514 398 6294.
E-mail address: mary.fiorilli@mcgill.ca (M.P. Païdoussis).

0889-9746/$ - see front matter © 2007 Published by Elsevier Ltd.
doi:10.1016/j.jfluidstructs.2007.07.004

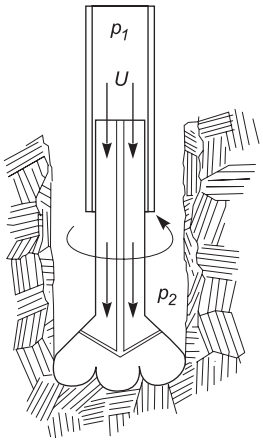

Fig. 1. Diagram of the drill-string and floating drill bit, rotating under the action of the flow (Den Hartog, 1969).

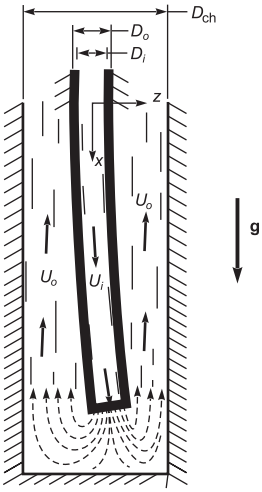

Fig. 2. The system under consideration, showing a long vertical tubular cantilever conveying fluid downwards; the fluid is then pushed upwards in the outer annular region contained by a rigid channel.

is lost by rubbing of the buckled string against the surrounding rock. In fact, this system also buckles, not as a result of axial compression, but by the effect of internal pressurization, as also discussed in Païdoussis (1998).

The system under consideration in this paper is a further idealization of the foregoing, essentially by ignoring the drill-bit altogether. So, this is no longer a realistic model for a drilling system; or it could be considered to be one relying wholly on erosion. Thus, we have a long tubular cantilever internally conveying fluid downwards; the fluid, after emerging from the free end, reverses direction and flows upwards in the annular region formed by the cantilever and an outer rigid channel, as shown diagrammatically in Fig. 2. Therefore, the study in this paper may be considered to be a fundamental investigation of the system of Fig. 2, inspired by drilling applications.

The problem of a cylindrical cantilever subjected concurrently to internal and external flows has been studied before, by Cesari and Curioni (1971), Hannoyer and Païdoussis (1978), Grigoriev (1978), Païdoussis and Besançon (1981), Luu (1983) and Wang and Bloom (1999). Of particular interest is Hannoyer and Païdoussis's (1978) study, combining theory and experiments on the linear dynamics and stability of a cylinder with supported ends or cantilevered, subject to both internal and external axial flows; a rich dynamical behaviour was revealed, involving multiple divergence and flutter instabilities. Theory and experiments were in quite good agreement.

Luu's (1983) thesis is the basis of the present paper. It differs from the work just cited in two significant ways: first, the two flows are countercurrent, and second they are not independent of each other. This work remained unpublished, until recent developments, briefly discussed below, provided a new impetus to sharing it with the wider research community.

The first element in this new impetus is related to the dynamics of aspirating pipes, of the type used, for instance, for ocean mining (Chung et al., 1981; Deepak et al., 2001). The see-saw path to understanding the dynamics of this system is related in Païdoussis et al. (2005). The system was originally thought to be subject to flutter at very small flow velocities—infinitesimally small in the absence of dissipation (Païdoussis and Luu, 1985). This was revised to suggest that the system is totally immune to instability (Païdoussis, 1998, 1999), and the problem was linked to Feynman's quandary on the sense of rotation of a hypothetical aspirating rotary sprinkler (Gleick, 1992); refer also to Pramila (1992). Doubts on the validity of the proof provided in Païdoussis (1999) were voiced by Kuiper and Metrikine (2005), suggesting that flutter is indeed *possible*. This forced a reevaluation of the problem in Païdoussis et al. (2005), modifying Kuiper and Metrikine's analysis, but nevertheless concluding that flutter may indeed be possible, the final answer depending on careful evaluation of the flow field close to the inlet, currently under CFD study. This brief account is perhaps too condensed for an interested but uninitiated reader to grasp fully; reference should be made to Païdoussis et al. (2005) and Païdoussis (2005) for a detailed discussion of the evaluation of understanding of this intriguing problem, and also to Kuiper and Metrikine (2006, 2008) for some new but perplexing experiments. In parallel, considerable work has been done on Feynman's "reverse sprinkler", the dynamics of which is fundamentally similar to that of the aspirating pipe; see, e.g., Forrester (1986), Hsu (1988), Berg and Collier (1989) and Creutz (2005).

For the system of Fig. 2, the cantilever is not aspirating, but it is nevertheless subjected to "reverse" external flow, i.e. from the free end towards the fixed one. Bearing in mind the similarities between the dynamics of cylinders subjected to internal and external axial flows (Païdoussis, 2004), it is indeed of interest to study the dynamics of a system subjected to "reverse" external flow, which corresponds to aspirating internal flow.

The second impetus comes from MEMS/nanotechnology, specifically the use of microcantilevers and microchannels for atomic force microscopy (AFM) and biomolecular detection [see, e.g., Putman et al., 1994; Burg and Manalis, 2003; Fukuma et al., 2005; Basak et al., 2006], in which it is important to devise cantilevers immersed in viscous fluid but nevertheless exhibiting very small damping. Clearly, that can be achieved for a cantilever subject to a flow-induced Hopf bifurcation at flow rates inferior but close to the critical value. This will be explored specifically and more fully in another paper, but it has nevertheless served to revitalize interest in the topic of this paper.

The present paper undertakes the first, linear study of the idealized system shown in Fig. 2. In keeping with the problem which inspired this study in the first place, the system considered resembles that of a drill-string, namely it is vertical and long and hence quite pliable. However, qualitatively the dynamics is the same for shorter cantilevers, as will be demonstrated by sample calculations for a bench-top-size system.

2. Derivation of the equation of motion

The system under consideration consists of a uniform tubular cantilever beam of length L, external cross-sectional area A_o, mass per unit length M_t and flexural rigidity EI, conveying downwards incompressible fluid of mass per unit length M_f, flowing axially with velocity U_i. The fluid leaving the free end of the tubular beam is then pushed upwards with velocity U_o within an outer rigid channel. The internal and external cross-sectional flow areas are A_f and A_{ch}, respectively; the fluid pressures, measured above the atmospheric, are p_i and p_o, respectively, for the inside and outside flow regions. The internal and external flow velocities, U_i and U_o, respectively, are therefore related to each other; their specific relation will be expressed later on. The tube axis in its undeformed (equilibrium) state coincides with the x-axis (Fig. 2).

Consider a small element of the tubular beam, of length δx, as shown in Fig. 3, under the action of structural and fluid-related forces and moments. Force balances in the x- and z-directions give

$$\frac{\partial T}{\partial x}-\frac{\partial}{\partial x}\left(Q\frac{\partial w}{\partial x}\right)+M_t g+F_{it}-F_{et}-(F_{in}+F_{en})\frac{\partial w}{\partial x}=0 \tag{1}$$

and

$$\frac{\partial Q}{\partial x}+\frac{\partial}{\partial x}\left(T\frac{\partial w}{\partial x}\right)+F_{in}+F_{en}+(F_{it}-F_{et})\frac{\partial w}{\partial x}-M_t\frac{\partial^2 w}{\partial t^2}=0, \tag{2}$$

where Q is the transverse shear force in the tubular beam, T is the axial tension, F_{in}, F_{it} are, respectively, the normal and tangential hydrodynamic forces due to the internal flow, F_{en}, F_{et} are, respectively, the normal and tangential hydrodynamic forces due to the external flow, and w is the lateral deflection.

From Euler–Bernoulli beam theory, one has

$$Q=-\frac{\partial}{\partial x}\left(EI\frac{\partial^2 w}{\partial x^2}\right). \tag{3}$$

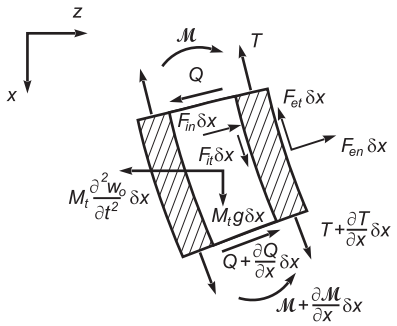

Fig. 3. Forces and moments acting on an element δx of the tubular cantilever.

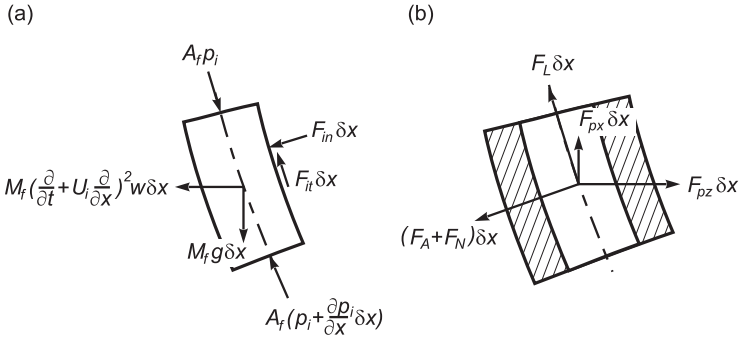

Fig. 4. (a) Forces acting on an element δx of the internally flowing fluid. (b) Forces due to the outside flow acting on the external surface of an element δx of the tubular cantilever.

Substituting relation (3) into Eqs. (1) and (2), and neglecting second-order terms, gives

$$\frac{\partial T}{\partial x}+F_{it}-F_{in}\frac{\partial w}{\partial x}-F_{et}-F_{en}\frac{\partial w}{\partial x}+M_t g=0 \tag{4}$$

and

$$EI\frac{\partial^4 w}{\partial x^4}-\frac{\partial}{\partial x}\left(T\frac{\partial w}{\partial x}\right)-F_{in}-F_{it}\frac{\partial w}{\partial x}-F_{en}+F_{et}\frac{\partial w}{\partial x}+M_t\frac{\partial^2 w}{\partial t^2}=0. \tag{5}$$

2.1. Hydrodynamic forces F_{in} and F_{it} due to the internal flow

Consider the forces acting on an element of the fluid enclosed within the tube element of Fig. 3, as shown in Fig. 4(a). The rate of change of fluid momentum per unit length is $M_f[(\partial/\partial t)+U_i(\partial/\partial x)]^2 w$ and zero in z- and x-directions, respectively (Gregory and Païdoussis, 1966a; Païdoussis, 1998, Section 3.3.2). Therefore, force balances in the x- and z-directions give, respectively,

$$F_{it}-F_{in}\frac{\partial w}{\partial x}=M_f g-A_f\frac{\partial p_i}{\partial x} \tag{6}$$

and

$$-F_{in}-F_{it}\frac{\partial w}{\partial x}=M_f\left(\frac{\partial^2 w}{\partial t^2}+2U_i\frac{\partial^2 w}{\partial x\,\partial t}+U_i^2\frac{\partial^2 w}{\partial x^2}\right)+A_f\frac{\partial}{\partial x}\left(p_i\frac{\partial w}{\partial x}\right). \tag{7}$$

2.2. Hydrodynamic forces F_{en}, F_{et} due to the external flow

As shown in Fig. 4(b), the hydrodynamic forces F_{en} and F_{et} due to the external (annular) flow consist of

(i) F_A, the lateral inviscid hydrodynamic force,
(ii) F_{px}, F_{pz}, the forces due to the outside mean pressure and gravity, and
(iii) F_N, F_L, the frictional viscous forces.

These will be discussed separately in what follows.

2.2.1. The inviscid hydrodynamic force

As shown by Hannoyer and Païdoussis (1978)—see also Païdoussis (2004)—the lateral inviscid hydrodynamic force per unit length has the form

$$F_A = \chi\left(\frac{\partial}{\partial t} - U_o\frac{\partial}{\partial x}\right)\left[\rho_f A_o\left(\frac{\partial w}{\partial t} - U_o\frac{\partial w}{\partial x}\right)\right], \tag{8}$$

where $\chi\rho_f A_o$ is the added (hydrodynamic) mass per unit length for the annular flow in this work, $\rho_f A_o$ being the displaced mass of fluid per unit length, and

$$\chi = \frac{(D_{ch}/D_o)^2 + 1}{(D_{ch}/D_o)^2 - 1}, \tag{9}$$

where D_o is the outer diameter of the pipe and D_{ch} the inner diameter of the channel (Fig. 2); so that $\chi > 1$.

2.2.2. The forces F_{px} and F_{pz} due to the mean pressure and gravity

Assuming that the outer pressure (in the annulus) p_o varies with x linearly, hydrostatically as well as because of frictional pressure losses, one can find (Hannoyer and Païdoussis, 1978; Païdoussis, 2004)

$$F_{px} = -\frac{\partial}{\partial x}(A_o p_o) + A_o\frac{\partial p_o}{\partial x}, \tag{10}$$

$$F_{pz} = A_o\frac{\partial}{\partial x}\left(p_o\frac{\partial w}{\partial x}\right). \tag{11}$$

Here, $F_{px} = 0$ since $\mathrm{d}A_o/\mathrm{d}x = 0$; but F_{px} is kept in this form for convenience.

The outside mean pressure p_o may now be obtained by considering a force balance of the flow in the annular region (Fig. 5) of length Δx:

$$-A_{ch}\frac{\mathrm{d}p_o}{\mathrm{d}x}\Delta x + F_f\Delta x + A_{ch}\rho_f g\Delta x = 0, \tag{12}$$

where p_o has been assumed to be uniform across the cross-sectional area $A_{ch} = \frac{1}{4}\pi(D_{ch}^2 - D_o^2)$, and F_f, the total frictional force, is

$$F_f = F_L\left(\frac{S_{\mathrm{tot}}}{S_o}\right), \tag{13}$$

in which F_L is the longitudinal frictional viscous force per unit length, to be discussed in the next section, $S_{\mathrm{tot}} \equiv \pi D_{ch} + \pi D_o$ is the total wetted area per unit length, and S_o the outside wetted area per unit length of the tube.

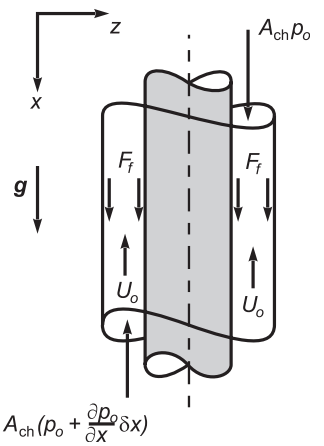

Fig. 5. Forces acting on an element δx of the annular flow contained by the tubular cantilever on the one side and the rigid channel on the other.

Combining Eqs. (12) and (13) and integrating the resultant equation with respect to x gives

$$A_o p_o = \left(A_o \rho_f g + F_L \frac{D_o}{D_h} \right) x, \tag{14}$$

where the exit pressure at surface level ($x = 0$) is assumed to be zero, and $D_h (\equiv 4A_{ch}/S_{\text{tot}})$ is the hydraulic diameter of the annular channel flow.

2.2.3. Frictional viscous forces F_N, F_L and dissipation in the tubular beam

Using the expressions proposed by Taylor (Taylor, 1952) in their modified form (Païdoussis, 1973, 2004), the frictional viscous forces in the normal and tangential directions are given by[1]

$$\begin{aligned} F_N &= \frac{1}{2} C_f \rho_f D_o U_o \left(\frac{\partial w}{\partial t} - U_o \frac{\partial w}{\partial x} \right) + k \frac{\partial w}{\partial t}, \\ F_L &= \tfrac{1}{2} C_f \rho_f D_o U_o^2, \end{aligned} \tag{15}$$

where C_f and k are the viscous damping coefficients. It is realized that the superposition in F_N of the viscous forces associated with (i) the mean axial flow and (ii) a quiescent fluid is an approximation—likely resulting in an overestimation of the actual viscous force. The alternative is a full viscous flow calculation, not a trivial task and one not deemed to be justified for the purposes of this paper. In any case, the approach adopted here has been shown to yield results in reasonable agreement with experiment for similar physical situations (Païdoussis, 2004).

The following expression is used for the viscous damping coefficient k:

$$k = \frac{2\sqrt{2}}{\sqrt{S}} \frac{1 + \overline{\gamma}^3}{(1 - \overline{\gamma}^2)^2} \rho_f A_o \Omega, \tag{16}$$

where $S = \Omega r_o^2 / \nu$ is the Stokes number, Ω being the circular frequency of oscillation, $r_o = \frac{1}{2} D_o$, and ν the kinematic viscosity of the fluid; $\overline{\gamma} = D_o / D_{ch}$, with D_o and D_{ch} as defined in Fig. 2 (Sinyavskii et al., 1980; Païdoussis, 1998). For $\overline{\gamma} \to 0$, this expression is identical to that derived in different ways by Batchelor (1967) and Chen (1981), valid for unconfined flow.[2] Eq. (16) is valid for $S \gg 1$, and it has been confirmed to give results in good agreement with the fuller analysis of Chen et al. (1976).

For the frictional damping coefficient C_f, the semi-empirical value of $C_f = 0.0125$ is used (Hannoyer and Païdoussis, 1978; Païdoussis, 2004).

Finally, it is noted that dissipation also occurs due to internal friction in the material of the tubular beam. This may be taken into account by assuming that it is entirely a hysteretic effect, thus considering the Young's modulus to be complex: $E(1 + \overline{\mu}\mathrm{i})$, where $\overline{\mu} \ll 1$. Alternatively, it could be represented by a viscoelastic model, e.g. replacing the flexural force $EI(\partial^4 w/\partial x^4)$ in Eq. (5) by $[E + E^*(\partial/\partial t)]I(\partial^4 w/\partial x^4)$. However, for the problem at hand, as the viscous damping due to the surrounding fluid is quite large, this form of dissipation will be neglected.

2.2.4. The equation of motion

Using relations (8), (10) and (11), one may write, correctly to the first order (Fig. 3),

$$-F_{et} - F_{en} \frac{\partial w}{\partial x} = -F_L + \frac{\partial}{\partial x}(A_o p_o) - A_o \frac{\partial p_o}{\partial x}, \tag{17}$$

$$-F_{en} + F_{et} \frac{\partial w}{\partial x} = \chi \left(\frac{\partial}{\partial t} - U_o \frac{\partial}{\partial x} \right) \left[\rho_f A_o \left(\frac{\partial w}{\partial t} - U_o \frac{\partial w}{\partial x} \right) \right] - A_o \frac{\partial}{\partial x} \left(p_o \frac{\partial w}{\partial x} \right) + F_N + F_L \frac{\partial w}{\partial x}, \tag{18}$$

where F_N and F_L are given by Eqs. (15).

[1] In the original form of this analysis (Luu, 1983), the first term in F_N reads $-\frac{1}{2} C_f \rho_f D_o U_o [(\partial w/\partial t) - U_o(\partial w/\partial x)]$, obtained by simply replacing U_o for downwards flow to $-U_o$ for upwards flow throughout. However, this is now believed to be wrong; in the final equation, Eq. (21), it would result in negative damping for lateral motions of the system [the penultimate term in Eq. (21) would have a minus in front of it].

[2] In Luu (1983), the expression for $\overline{\gamma} = 0$ was used in the calculations, thus severely underestimating this viscous damping effect.

The equation of motion may be obtained by substituting Eqs. (7) and (18) into Eq. (5) to give

$$EI\frac{\partial^4 w}{\partial x^4}-\frac{\partial}{\partial x}\left[(T-A_f p_i+A_o p_o)\frac{\partial w}{\partial x}\right]+F_N+F_L\frac{\partial w}{\partial x}+M_t\frac{\partial^2 w}{\partial t^2}$$
$$+M_f\left(\frac{\partial^2 w}{\partial t^2}+2U_i\frac{\partial^2 w}{\partial x\,\partial t}+U_i^2\frac{\partial^2 w}{\partial x^2}\right)+\chi\rho_f A_o\left(\frac{\partial^2 w}{\partial t^2}-2U_o\frac{\partial^2 w}{\partial x\,\partial t}+U_o^2\frac{\partial^2 w}{\partial x^2}\right)=0, \tag{19}$$

where $(T-A_f p_i+A_o p_o)$ may be determined by substituting expressions (6), (14), (15) and (17) into (4), yielding

$$\frac{\partial}{\partial x}(T-A_f p_i+A_o p_o)+(M_t+M_f-\rho_f A_o)g-\frac{1}{2}C_f\rho_f D_o U_o^2\left(1+\frac{D_o}{D_h}\right)=0,$$

which, after being integrated from x to L, becomes

$$(T-A_f p_i+A_o p_o)=(T-A_f p_i+A_o p_o)_L+(M_t+M_f-\rho_f A_o)g(L-x)$$
$$-\frac{1}{2}C_f\rho_f D_o U_o^2\left(1+\frac{D_o}{D_h}\right)(L-x). \tag{20}$$

Hence, the final form of the equation of motion may now be obtained by combining Eqs. (19) and (20),

$$EI\frac{\partial^4 w}{\partial x^4}+M_t\frac{\partial^2 w}{\partial t^2}+M_f\left(\frac{\partial^2 w}{\partial t^2}+2U_i\frac{\partial^2 w}{\partial x\,\partial t}+U_i^2\frac{\partial^2 w}{\partial x^2}\right)+\chi\rho_f A_o\left(\frac{\partial^2 w}{\partial t^2}-2U_o\frac{\partial^2 w}{\partial x\,\partial t}+U_o^2\frac{\partial^2 w}{\partial x^2}\right)$$
$$-\left[(T-A_f p_i+A_o p_o)_L+(M_t+M_f-\rho_f A_o)g(L-x)-\frac{1}{2}C_f\rho_f D_o U_o^2\left(1+\frac{D_o}{D_h}\right)(L-x)\right]\frac{\partial^2 w}{\partial x^2}$$
$$+\left[(M_t+M_f-\rho_f A_o)g-\frac{1}{2}C_f\rho_f D_o U_o^2\left(1+\frac{D_o}{D_h}\right)\right]\frac{\partial w}{\partial x}+\frac{1}{2}C_f\rho_f D_o U_o\frac{\partial w}{\partial t}+k\frac{\partial w}{\partial t}=0. \tag{21}$$

The only terms yet undefined are p_{iL} and p_{oL}. Assuming a smooth transition between internal and annular flows at the lower end of the system, one may use the simplified relationship

$$p_{iL}+\tfrac{1}{2}\rho_f U_i^2=p_{oL}+\tfrac{1}{2}\rho_f U_o^2+\rho_f g h_o, \tag{22}$$

where h_o is the loss of head that arises due to the sudden enlargement in the flow areas from A_f to A_{ch}; this may be expressed in the form

$$h_o=\frac{1}{2g}C(U_i-U_o)^2 \tag{23}$$

and we take $C=1$; see, e.g., Idel'chik (1986).

Substituting Eq. (23) into Eq. (22) and rearranging terms, finally gives

$$p_{iL}=p_{oL}+\rho_f U_o(U_o-U_i), \tag{24}$$

where p_{oL} may be calculated from expression (14) to be

$$p_{oL}=[\rho_f g+(F_L/A_o)(D_o/D_h)]L. \tag{25}$$

A final word on the equation of motion just derived relates to the fact that it is for planar, two-dimensional (2-D) motions. Yet, it is known that flutter in external axial flow manifests itself typically as an orbital 3-D motion (Païdoussis et al., 2002). Also, flutter of pipes conveying fluid is often 3-D (Bajaj and Sethna, 1984). In general, since the flow at inlet is irrotational, 3-D motions are associated with nonlinear coupling in the curvature of the oscillating cylinder, although for external flow the fluid may acquire a rotary component by other means. In experiments, flutter begins in a plane, but may become orbital by the time a limit-cycle motion is established. In theoretical computations, in any case, whether one imposes 2-D motions in a 3-D model or allows 3-D motions, the *critical* flow velocities for instability are the same. Hence, for the linear analysis in this paper, a 2-D model is sufficient.

2.2.5. Boundary conditions

The equation of motion (21) is subjected to the boundary conditions

$$w(0,t)=\left.\frac{\partial w}{\partial x}\right|_{x=0}=0,\quad \left.\frac{\partial^2 w}{\partial x^2}\right|_{x=L}=\left.\frac{\partial^3 w}{\partial x^3}\right|_{x=L}=0. \tag{26}$$

Of course, the assumption of zero shear at the free end is an idealized condition, effectively supposing that the fluid redistributes itself at the bottom of the well in Fig. 2, such that it flows wholly *uniformly* upwards around the

cylinder—at least prior to the onset of instability; a hemispherical shape for the bottom of the well would aid in this respect. Once motion begins, and one has to suppose an infinitesimally small motion to assess stability, the flow ceases being symmetric; lateral forces are generated, and possibly a shear force at the free end. This deserves being explored in any second-generation modelling of the problem.

3. Dimensionless equation of motion and boundary conditions

Before proceeding with the analysis, it is convenient to render the system of equations nondimensional by the use of the following dimensionless quantities:

$$\xi = x/L, \quad \eta = w/L, \quad \tau = [EI/(M_t + M_f + \rho_f A_o)]^{1/2} t/L^2,$$
$$u_i = (M_f/EI)^{1/2} U_i L, \quad u_o = (\rho_f A_o/EI)^{1/2} U_o L, \quad \beta_o = \rho_f A_o/(M_t + M_f + \rho_f A_o),$$
$$\beta_i = M_f/(M_t + M_f + \rho_f A_o), \quad \gamma = (M_t + M_f - \rho_f A_o) g L^3/EI, \quad \Gamma = T_L L^2/EI,$$
$$\Pi_{iL} = p_{iL} A_f L^2/EI, \quad \Pi_{oL} = p_{oL} A_o L^2/EI, \quad c_f = 4C_f/\pi, \quad \kappa = kL^2/[EI(M_t + M_f + \rho_f A_o)]^{1/2},$$
$$\varepsilon = L/D_o, \quad h = D_o/D_h, \quad \alpha = D_i/D_o, \quad \alpha_{ch} = D_{ch}/D_o. \tag{27}$$

Substituting Eqs. (27) into Eq. (21)

$$\frac{\partial^4 \eta}{\partial \xi^4} + [1 + \beta_o(\chi - 1)] \frac{\partial^2 \eta}{\partial \tau^2} + 2(u_i \beta_i^{1/2} - \chi u_o \beta_o^{1/2}) \frac{\partial^2 \eta}{\partial \xi \, \partial \tau} + (u_i^2 + \chi u_o^2) \frac{\partial^2 \eta}{\partial \xi^2}$$
$$- \left[(\Gamma - \Pi_{iL} + \Pi_{oL}) + \gamma(1 - \xi) - \frac{1}{2} c_f \varepsilon u_o^2 (1 + h)(1 - \xi) \right] \frac{\partial^2 \eta}{\partial \xi^2}$$
$$+ \left[\gamma - \frac{1}{2} c_f \varepsilon u_o^2 (1 + h) \right] \frac{\partial \eta}{\partial \xi} + \frac{1}{2} c_f \varepsilon u_o \beta_o^{1/2} \frac{\partial \eta}{\partial \tau} + \kappa \frac{\partial \eta}{\partial \tau} = 0. \tag{28}$$

The corresponding boundary conditions are

$$\eta(0, \tau) = \frac{\partial \eta}{\partial \xi}(0, \tau) = 0, \quad \frac{\partial^2 \eta}{\partial \xi^2}(1, \tau) = \frac{\partial^3 \eta}{\partial \xi^3}(1, \tau) = 0. \tag{29}$$

The relation of the pressures at the free end in expression (25) may now be written as

$$\Pi_{iL} = \alpha^2 \Pi_{oL} + \alpha u_o (\alpha u_o - u_i) \tag{30}$$

with $\Pi_{oL} = \rho_f A_o g L^3/EI + \frac{1}{2} c_f \varepsilon u_o^2 h$.

As already noted, the inside and outside flow velocities are related through continuity, i.e. $U_i A_f = U_o A_{ch}$, which after some manipulation may be expressed as

$$u_o = \frac{\alpha}{(\alpha_{ch}^2 - 1)} u_i \tag{31}$$

with u_i and u_o, the dimensionless inside and outside flow velocities, respectively, defined in Eq. (27), and $\alpha_{ch} = D_{ch}/D_o$.

Also, h, the ratio of the outside diameter to the hydraulic one ($D_h = 4A_{ch}/S_{\text{tot}}$) may be expressed in terms of α_{ch} as follows:

$$h = \left(\frac{\alpha_{ch} + 1}{\alpha_{ch}^2 - 1} \right). \tag{32}$$

As the lower end of the tubular beam is considered to be free, any externally imposed tension must be zero ($\Gamma = 0$).

4. Methods of solution

Two methods of solution have been used. The first is a hybrid Galerkin–Fourier method, which proved to be quite efficient. The second is the conventional Galerkin method.

4.1. The hybrid Galerkin–Fourier method

The method is first outlined in general, for any beam or beam-like structure subjected to fluid loading, and then for the particular problem at hand.

We consider free motions, and we separate variables in the equation of motion by seeking solutions of the form

$$\eta(\xi,\tau) = \Psi(\xi)\,\mathrm{e}^{\mathrm{i}\omega\tau}, \tag{33}$$

where ω is a dimensionless complex frequency. Clearly, stability or instability may be assessed accordingly as the imaginary component of ω is positive or negative. Substituting into Eq. (28) and into the four boundary conditions (29), we obtain a set of ordinary differential equations of the form

$$\sum_{r=0}^{4} f_r(\xi,\omega)\frac{\mathrm{d}^r\Psi}{\mathrm{d}\xi^r} = 0, \tag{34}$$

and

$$\sum_{r=0}^{3} g_r^j(\omega)\left[\frac{\mathrm{d}^r\Psi}{\mathrm{d}\xi^r}\right]_{\xi=\xi_j} = 0, \quad j = 1,2,3,4, \quad \xi_1 = \xi_2 = 0, \quad \xi_3 = \xi_4 = 1, \tag{35}$$

where in this particular case the $g_r^j(\omega)$ are all equal to unity.

The solution of these equations is accomplished by a Galerkin-like method, utilizing Fourier-series admissible functions (Hannoyer, 1972; see also Païdoussis, 2004, pp. 900–901). The periodicity of the series must be greater than unity, in order to satisfy the boundary conditions at $\xi = 0$ and $\xi = 1$ and to allow for the continuity of Ψ and its derivatives; for convenience, a periodicity of 2 is chosen, such that

$$\Psi(\xi) = \sum_{-\infty}^{\infty} a_n \frac{\mathrm{e}^{\mathrm{i}n\pi\xi}}{\sqrt{2}} = \sum_{0}^{\infty}\{\beta_{2n-1}\sin n\pi\xi + \beta_{2n}\cos n\pi\xi\}/\sqrt{2}, \tag{36}$$

where the β are complex. Hence, Eqs. (34) and (35) may now be written as follows:

$$D(\xi,\omega) \equiv \sum_{r=0}^{4} f_r(\xi,\omega)\frac{\mathrm{d}^r}{\mathrm{d}\xi^r}[\beta_{2n-1}\sin n\pi\xi + \beta_{2n}\cos n\pi\xi] = 0, \tag{37}$$

$$\sum_{r=0}^{3} g_r^j(\omega)\left\{\frac{\mathrm{d}^r}{\mathrm{d}\xi^r}\sum_{n=0}^{\infty}[\beta_{2n-1}\sin n\pi\xi + \beta_{2n}\cos n\pi\xi]\right\}_{\xi=\xi_j} = 0, \tag{38}$$

and we impose

$$\int_0^1 D(\xi,\omega)\sin p\pi\xi\,\mathrm{d}\xi = 0, \quad \int_0^1 D(\xi,\omega)\cos p\pi\xi\,\mathrm{d}\xi = 0, \quad p = 1,2,\ldots\ . \tag{39}$$

Each of Eqs. (39) yields a homogeneous relation between the β; the four boundary conditions (38) are also linear and homogeneous. Hence, all the equations may be written in the form

$$[A(\mathrm{i}\omega)]\{\beta\} = \{0\}; \tag{40}$$

the requirement for nontriviality yields a vanishing determinant, from which the values of ω may be obtained.

For the particular problem at hand, Eqs. (34) and (35) become

$$\begin{aligned}(1+\overline{\mu})\frac{\mathrm{d}^4\Psi}{\mathrm{d}\xi^4} &+ \left[u_i^2 + \chi u_o^2 - (\Gamma - \Pi_{iL} + \Pi_{oL}) - \gamma(1-\xi) + \frac{1}{2}c_f\varepsilon u_o^2(1+h)(1-\xi)\right]\frac{\mathrm{d}^2\Psi}{\mathrm{d}\xi^2}\\ &+ \left[\gamma - \frac{1}{2}c_f\varepsilon u_o^2(1+h) + 2\mathrm{i}\omega(u_i\beta_i^{1/2} - \chi u_o\beta_o^{1/2})\right]\frac{\mathrm{d}\Psi}{\mathrm{d}\xi}\\ &+ \left[\mathrm{i}\omega\left(\frac{1}{2}c_f\varepsilon u_o\beta_o^{1/2} + \kappa\right) - \omega^2(1 + \chi\beta_o - \beta_o)\right]\Psi = 0,\end{aligned} \tag{41}$$

$$\Psi(0) = \frac{\mathrm{d}\Psi}{\mathrm{d}\xi}(0) = 0, \quad \frac{\mathrm{d}^2\Psi}{\mathrm{d}\xi^2}(1) = \frac{\mathrm{d}^3\Psi}{\mathrm{d}\xi^3}(1) = 0. \tag{42}$$

Then, the particular forms of Eqs. (37) and (38) follow directly. For example, Eq. (38) becomes

$$\Psi(0) = \sum_{n=0}^{\infty} \frac{1}{\sqrt{2}} \{\beta_{2n-1} \sin n\pi\xi + \beta_{2n} \cos n\pi\xi\}_{\xi=0} = 0,$$

$$\frac{d\Psi}{d\xi}(0) = \left[\frac{d}{d\xi} \sum_{n=0}^{\infty} \frac{1}{\sqrt{2}} \{\beta_{2n-1} \sin n\pi\xi + \beta_{2n} \cos n\pi\xi\}\right]_{\xi=0} = 0,$$

$$\frac{d^2\Psi}{d\xi^2}(1) = \left[\frac{d^2}{d\xi^2} \sum_{n=0}^{\infty} \frac{1}{\sqrt{2}} \{\beta_{2n-1} \sin n\pi\xi + \beta_{2n} \cos n\pi\xi\}\right]_{\xi=1} = 0,$$

$$\frac{d^3\Psi}{d\xi^3}(1) = \left[\frac{d^3}{d\xi^3} \sum_{n=0}^{\infty} \frac{1}{\sqrt{2}} \{\beta_{2n-1} \sin n\pi\xi + \beta_{2n} \cos n\pi\xi\}\right]_{\xi=1} = 0. \tag{43}$$

The particular forms of Eqs. (39) and (40) are now rather obvious. They will not be given here explicitly, for brevity, but may be found in Luu (1983).

Convergence, for the results to be discussed in the next section, was found to be fast: the results with $n = 10$ and 11 differed by less than 1.3%.

4.2. The conventional Galerkin method

This method being very well known, there is no need to elaborate it; refer to Païdoussis (1998, Section 2.1.3), for example. In this case the cantilever beam eigenfunctions were used as comparison functions.

4.3. Comparison of the two methods of solution

It is of interest that 40 or more comparison functions were necessary to achieve convergence for the drill-string-like system in the case of the conventional Galerkin method.[3] This is because the system eigenfunctions in this case are not very much like those of the cantilever beam, mainly because of the very large gravity effect [$\gamma \sim \mathcal{O}(10^4)$]. For the bench-top type system, however, convergence was achieved with only 10 comparison functions. As mentioned in Section 4.1, the Fourier–Galerkin method was considerably more efficient, with convergence being achieved with only 11 terms for the drill-string-like system.

Finally, it should be mentioned that the results obtained by the two methods were found to be identical to within 5% for the lowest two modes, which provides added confidence in their validity.

5. Typical results

5.1. The drill-string-like system used in the calculations

The system considered is a very slender system, with $\alpha = 0.9$, $\varepsilon = 2 \times 10^3$, $\beta_0 = 0.303$, $\beta_i = 0.245$, $\gamma = 11.85 \times 10^3$. If this were a drilling system, these dimensionless parameters could correspond to the following dimensional quantities: $D_o = 0.50\,\text{m}$, $D_i = 0.45\,\text{m}$, $L = 1000\,\text{m}$, $E = 200 \times 10^9\,\text{N/m}^2$, $\rho_t = 7.83 \times 10^3\,\text{kg/m}^3$, $\rho_f = 998\,\text{kg/m}^3$.

As mentioned earlier, the viscous coefficient C_f (due to the external axial flow) is assigned the value of $C_f = 0.0125$. The viscous damping coefficient k (and hence κ) is calculated via Eq. (16) for the actual Ω in each mode and for each u_i corresponding to the computed $\mathscr{R}e(\omega)$, iteratively if need be. This means a different set of calculations for each mode; depending on the variability of $\mathscr{R}e(\omega)$ with u_i, this could also mean a separate set of calculations for each u_i.

Finally, it is useful to note that, for the hypothetical drilling system considered, u_i and U_i (m/s) are related via

$$u_i = 0.867\, U_i. \tag{44}$$

[3]In the calculations for $\alpha_{ch} = 20$ involving high u_i, discussed in Section 5.2, it was found that more than 80 comparison functions were necessary.

5.2. Dynamics of the drill-string-like system and the effect of annular width

Here, it is of interest to discuss the effects on system stability of the internal and external axial flows, by varying u_i and hence u_o, and of the degree of narrowness of the annular region. Although the effect of small internal flow (i.e., u_i slightly larger than zero) is to damp the motion (Gregory and Païdoussis, 1966a, b; Païdoussis, 1970, 1998), the reverse external axial flow, by analogy to reverse internal flow, has the tendency to destabilize the system even for low u_o (Païdoussis et al., 2005); these qualitative aspects of the dynamics will be discussed further in Section 6. Here, the relative effect of u_i, u_o and the confinement of the outer annular region on the stability of the system can most conveniently be examined by varying just the system parameter α_{ch} ($\equiv D_{ch}/D_o$). A specific value of α_{ch} defines clearly the confinement of the outside annular region and hence determines the importance of the outside axial flow u_o with respect to the internal flow u_i (by means of Eq. (31)).

First, let us analyse the dynamics of the system with $\alpha_{ch} = 20$. For this geometrical arrangement, the external axial flow u_o is three orders of magnitude smaller than the internal flow u_i conveyed downwards in the tubular beam. It has been verified that the dynamical behaviour of the system with $\alpha_{ch} = 20$ is sensibly the same as that of a system with $\alpha_{ch} = 2 \times 10^3$ (where u_o is seven orders of magnitude smaller than u_i). Thus, for $\alpha_{ch} = 20$, the effect of the outside axial flow is negligible, as compared with the internal flow; hence, one can expect that the internal downward flow will dominate and will stabilize the system for small values of u_i.[4] In Fig. 6, the calculations have been carried out for the first three modes. Due to the viscous damping effect, the imaginary parts of the eigenfrequency ω_j, $\mathscr{I}m(\omega_j)$, are greater than zero at $u_i = 0$. As u_i is increased from zero, the $\mathscr{I}m(\omega_j)$ are increased, further stabilizing the system. Here, since the value of γ, which is nonzero for vertical tubular beams, is large ($\gamma \sim 10^4$), a very large internal downward flow velocity ($u_i \sim 100$) is necessary for the system to become unstable; calculations in Fig. 6 have not been taken to such high u_i. It may then be said that, for $\alpha_{ch} = 20$, the system is effectively stabilized by the internal flow. Flutter at $u_i \sim 100$ corresponds to too high a flow velocity ($U_i \simeq 1.15 u_i$) to be of practical interest.

Calculations for $\alpha_{ch} = 2$ display the same dynamical behaviour, at least for $u_i \leqslant 0.6$. Although in this case the external flow velocity $u_o = 0.3 u_i$, so quite appreciable, the dynamics is again dominated by the internal flow, and the effect of relatively small flow is to stabilize the system.

Next, the ratio of channel- to external-tube-diameter, α_{ch}, is reduced to $\alpha_{ch} = 1.2$ (i.e., $D_{ch}/D_o = 1.2$). In this case, the outer annular region is rather confined and the outside flow velocity u_o is of the same order of magnitude as u_i ($u_o = 2.045\ u_i$); hence one expects the effect of external flow to be at least as important as that of internal flow. The first three modes of the system (again with u_i as the variable) are shown in the Argand diagram of Fig. 7. The loci of the second and third modes in this case just go straight down [i.e., the $\mathscr{I}m(\omega_j)$ decrease] with increasing values of u_i, but that of the first mode remains essentially static (in the scale of this figure) in this velocity range.[5] The system loses stability in its second mode at $u_i \simeq 2.125$ at slightly lower flow velocity than the third mode (at $u_i \simeq 2.55$). Hence, for $\alpha_{ch} = 1.2$, the outside axial flow velocity, u_o, has a more dominant effect on the dynamics of the system than expected; it gives the system a net destabilizing action immediately, regardless of the damping effect of the internal downward flow u_i. Therefore, from the practical viewpoint, $\alpha_{ch} = 1.2$ represents a strongly confined system.

Here, comparing Fig. 7 to Fig. 6, it is also noted that the natural frequencies of the system [i.e., $\mathscr{R}e(\omega_j)$, $j = 1, 2, \ldots$] are smaller than those for $\alpha_{ch} = 20$; this is due to the fact that, with greater confinement by the rigid outer channel, the virtual (added) mass of the system is increased, and the natural frequencies of the system are thus decreased. It is further noted that the $\mathscr{I}m(\omega_j)$ for $u_i = 0$ are larger by one order of magnitude for $\alpha_{ch} = 1.2$ as compared to $\alpha_{ch} = 20$, indicating a sharp increase in damping due to confinement.

It is then of interest to see how the system behaves as the outside region is confined further (e.g., $\alpha_{ch} = 1.1$ and $u_o \simeq 4.28\, u_i$). This may appear to merely be an academic exercise, as for $\alpha_{ch} = 1.2$ the dimensional critical flow velocity is already very small (for a system with such a large value of γ); however, this is also of practical interest for real oil drilling systems, which may also have very small confinement in the outside annular region. As shown in Fig. 8, for a given increment of the internal flow velocity, u_i, the imaginary parts of the first three eigenfrequencies $\mathscr{I}m(\omega_j)$, $j = 1, 2, 3$, decrease much more rapidly than for the corresponding modes in the case of $\alpha_{ch} = 1.2$. The instability again occurs first in the second mode at $u_i = 0.96$ and is closely followed by the third and first modes. The real parts of the eigenfrequencies $\mathscr{R}e(\omega_j)$, $j = 1, 2, \ldots$, are further reduced in this case, as the $\mathscr{I}m(\omega_j)$ are further increased, at $u_i = 0$.

Clearly there are two opposing mechanisms at play as α_{ch} is reduced, in the range of α_{ch} in Figs. 7 and 8. The first is associated with the increase in u_o, which is destabilizing. The second is associated with the increase in flow-independent

[4] In this context, "small" for $\gamma = 0$ would be $u_i < 3$ approximately (Gregory and Païdoussis, 1966a); for $\gamma = 100, u_i < 6-8$ (Païdoussis, 1970). For the large γ here under consideration, "small" would easily be of $\mathcal{O}(50)$.

[5] By comparing Figs. 6 and 8, it becomes clear that the evolution of the first mode in Fig. 7 represents a transition between the first-mode locus moving up and moving down.

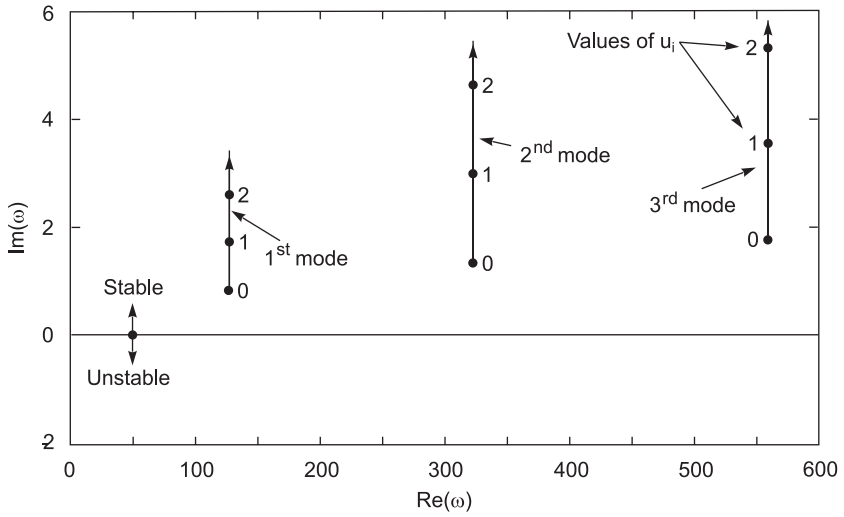

Fig. 6. Argand diagram of the complex dimensionless eigenfrequencies of the drill-string-like system, ω_i, $i = 1, 2, 3$, as a function of the dimensionless flow velocity u_i for $\alpha_{ch} = 20$.

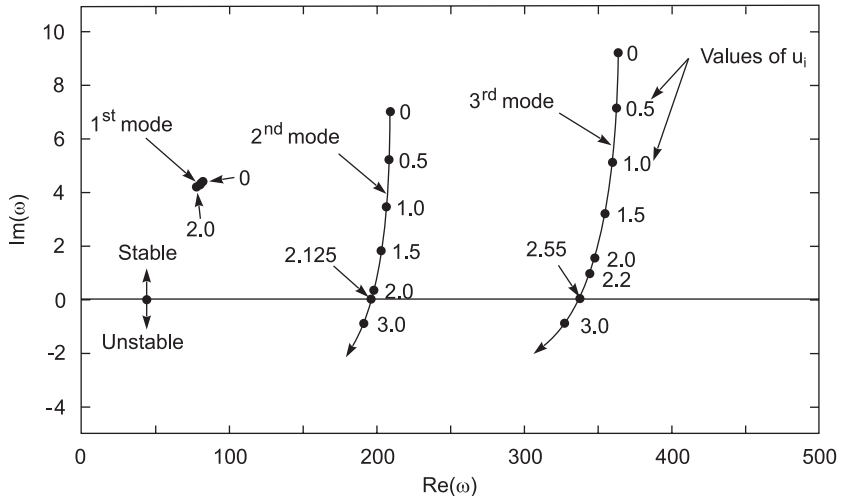

Fig. 7. Argand diagram of the complex dimensionless eigenfrequencies of the drill-string-like system, ω_i, $i = 1, 2, 3$, as a function of the dimensionless flow velocity u_i for $\alpha_{ch} = 1.2$.

viscous damping (higher values of κ) due to confinement, which is stabilizing—thus moving the $\mathscr{I}m(\omega_j)$ higher and therefore requiring a larger u_i to precipitate instability than would otherwise be the case.

The critical values of the internal downward flow velocities u_i, denoted as u_{icf}, in the case of small confinement of the outer annular region are summarized in Table 1.

Summarizing, it may be said that, with water as the flowing fluid, it has been shown that for $\alpha_{ch} \leqslant 1.2$, the external upward flow in the annular region plays a dominant role and has a net destabilizing effect on the system for $u_i > 0$. If no viscous damping is taken into account (i.e., with no dissipative effects), the system would have become unstable promptly for very small $u_i > 0$. Furthermore, it is noted that by decreasing α_{ch}, the dimensionless frequencies of oscillation, $\mathscr{R}e(\omega_j)$, are diminished, due to the larger virtual (added) mass existing in the system; the $\mathscr{I}m(\omega_j)$ at $u_i = 0$ are correspondingly increased because of the increasing narrowing of the annulus (increasing confinement).

Additional calculations have been made with air as the flowing fluid, so as to find out whether in this case the outside upward flow in the confined region has a smaller destabilizing effect on the dynamics of the problem. (A constant air density of $\rho_f = 1.21\,\mathrm{kg/m^3}$ was assumed throughout, for both internal and external flows, which, it is realized, is

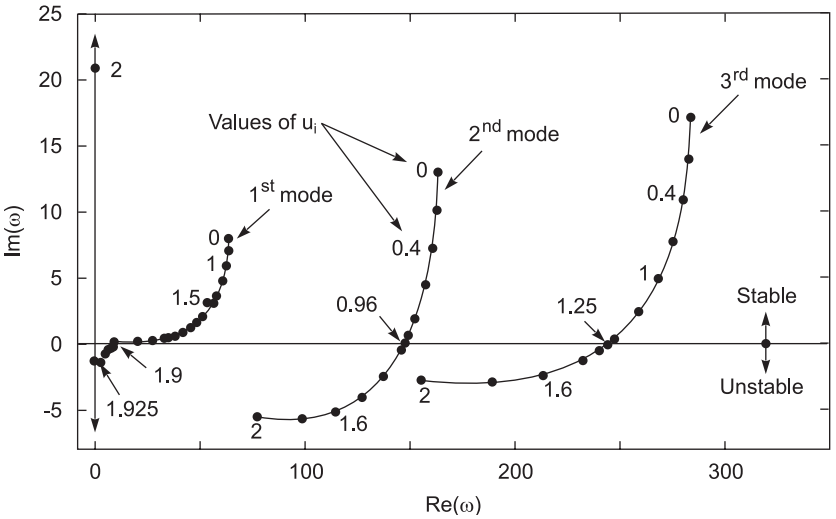

Fig. 8. Argand diagram of the complex dimensionless eigenfrequencies of the drill-string-like system, ω_i, $i = 1, 2, 3$, as a function of the dimensionless flow velocity u_i for $\alpha_{ch} = 1.1$.

Table 1
The critical flow velocities of the drill-string-like system under consideration, showing the effect of α_{ch} and of the fluid conveyed

Fluid	α_{ch}	u_{icf}		
		First mode	Second mode	Third mode
Water	1.2	–	2.12	2.55
Water	1.1	1.9	0.96	1.25
Air	1.2	1.5	0.25	0.25

unrealistic.) The results for $\alpha_{ch} = 1.2$ show that the behaviour of this system is similar to that obtained for water flow in Fig. 7, but the effects are more pronounced here; the instability occurs promptly in the second mode at $u_{icf} \simeq 0.25$ and almost simultaneously in the third mode. This is due to the fact that viscous damping, which is proportional to ρ_f, is 10^3 times smaller than the corresponding one of water flow; hence, in this case, the imaginary parts of the eigenfrequencies, $\mathcal{I}m(\omega_j)$, $j = 1, 2, 3$, are much closer to the neutral stability axis than the corresponding ones in Fig. 7, and instability occurs at much lower dimensionless flow velocities in air (see Table 1). In other words, if no viscous damping were included in the analysis, the system would become unstable for very small $u_i > 0$, for both air and water flows.

Finally, before closing this section, a major assumption inherent in all the foregoing work should be discussed, namely that there is no contact between the bottom of the pipe and the drill-bit, and hence no contact with the "ground". If temporary "contact" is assumed, the tubular beam will at that instant behave approximately as if it were pinned (simply-supported) at the bottom. If the system "sticks" to the wall more permanently, say as a result to imperfection-related bowing, its dynamics would clearly be affected, and stability would be lost by static divergence (Païdoussis, 1980, 2004; Zhang and Miska, 2005).

5.3. Dynamics of a bench-top-size system

The dynamics of a bench-top-size system has also been studied—a system involving an elastomer pipe ($E = 2.56 \times 10^6\,\mathrm{N/m^2}$) with dimensions such as might be pertinent for a bench-top experiment ($D_o = 15.7\,\mathrm{mm}$, $D_i = 6.4\,\mathrm{mm}$ and $L = 443\,\mathrm{mm}$, in a vertical arrangement otherwise similar to that for the drill-string-like system. The corresponding dimensionless parameters are $\alpha = 0.408$, $\varepsilon = 28.2$, $\beta_o = 0.467$, $\beta_i = 0.0776$, $\gamma = 3.14$). Typical results are shown in Fig. 9 for $\alpha_{ch} = 2.0$ and Fig. 10 for $\alpha_{ch} = 1.2$.

In Fig. 9, it is seen that the system behaves similarly to the drill-string-like system for this value of α_{ch}: the system is stabilized in all three modes for small u_i. However, in this case we begin to see the curving of the loci of the second and

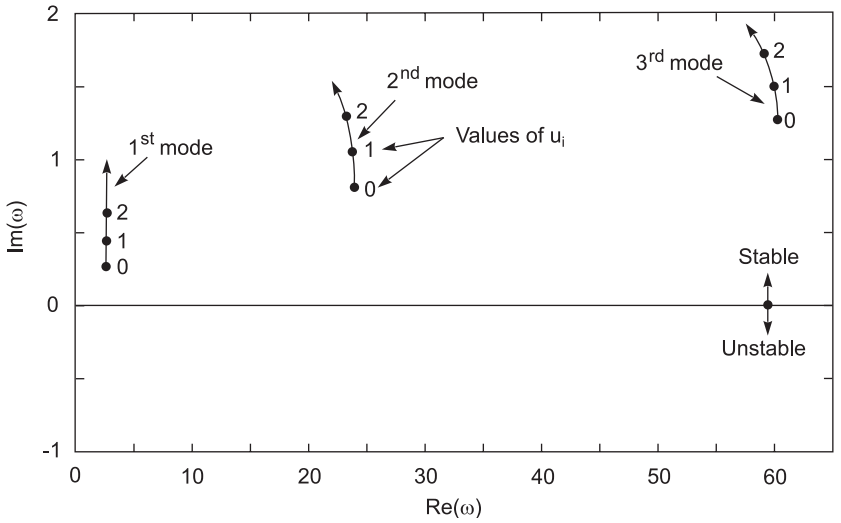

Fig. 9. Argand diagram of the complex dimensionless eigenfrequencies of the bench-top-size system, ω_i, $i = 1, 2, 3$, as a function of the dimensionless flow velocity u_i for $\alpha_{ch} = 2.0$.

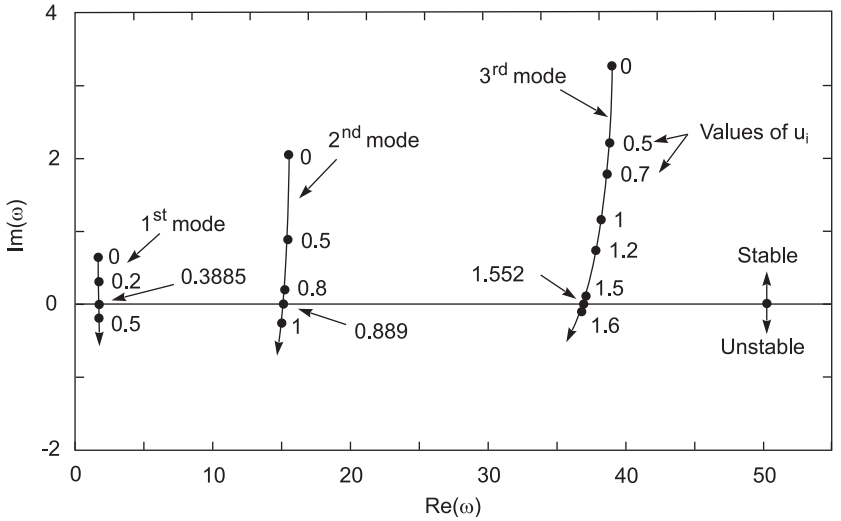

Fig. 10. Argand diagram of the complex dimensionless eigenfrequencies of the bench-top-size system, ω_i, $i = 1, 2, 3$, as a function of the dimensionless flow velocity u_i for $\alpha_{ch} = 1.2$.

Table 2
The critical flow velocities of the bench-top-size system, showing the effect of α_{ch} and of the pipe wall thickness

Pipe	α_{ch}	u_{icf}		
		First mode	Second mode	Third mode
Thick-walled ($D_i = 6.4$ mm)	20	–[a]	6.8	–[a]
	1.2	0.39	0.89	1.55
	1.1	0.27	0.61	1.03
Thin-walled ($D_i = 9.525$ mm)	1.2	0.25	0.60	1.0

[a]For $u_i \leqslant 10$, at least.

third modes, which eventually would cause them (or one of them, at any rate) to approach and eventually cross the neutral axis to instability.

A further calculation with $\alpha_{ch} = 20$ (essentially unconfined external flow) was carried out. In that case, the second mode reaches a maximum value of $\mathscr{I}m(\omega_2) \simeq 3$ at $u_i \simeq 5$. It then begins to decrease and crosses the neutral axis at $u_{icf} = 6.8$, at which point $\mathscr{R}e(\omega_2) = 14.2$.

The results for $\alpha_{ch} = 1.2$ are shown in Fig. 10. In this case the loci of the three modes go straight down. Stability is lost in the first mode ($u_i \simeq 0.39$), and at higher flows in the second and third modes, as tabulated in Table 2.

Calculations for $\alpha_{ch} = 1.1$ show the same trends. Instability first occurs again in the first mode and then in the other modes, as shown in Table 2.

Calculations were also done with a pipe of smaller wall thickness ($D_o = 15.7\,\text{mm}$, $D_i = 9.525\,\text{mm}$; $\beta_o = 0.474$, $\beta_i = 0.174$, $\varepsilon = 28.2$, $\gamma = 2.377$) and $\alpha_{ch} = 1.2$. The system behaves similarly to that for $\alpha_{ch} = 1.2$ and 1.1 and a thicker pipe, as seen in Table 2.

6. Qualitative dynamics

The objective here is to consider the mechanisms underlying the dynamical behaviour, as computed in the foregoing, and to compare it to that of simpler systems previously studied.

Consider first the dynamics associated with the inside flow, for convenience ignoring the presence of the dense outside fluid and the damping associated thereto. It has been shown (Benjamin, 1961a) that the work done by the fluid on the pipe in the course of one period of oscillation is

$$\Delta W_i = -M_f U_i \int_0^T \left[\left(\frac{\partial w}{\partial t} \right)_L^2 + U_i \left(\frac{\partial w}{\partial t} \right)_L \left(\frac{\partial w}{\partial x} \right)_L \right] \mathrm{d}t, \tag{45}$$

where the subscript L refers to the free end of the system and i stands for "inside flow". It is clear that, if U_i is sufficiently small, the first term in the square brackets predominates, and hence $\Delta W_i < 0$; thus, oscillations are damped by the action of the flow. This is the behaviour illustrated in Fig. 6. On the other hand, for sufficiently large U_i, the second term predominates and, if $\overline{(\partial w/\partial t)_L (\partial w/\partial x)_L}$ is negative (which is the case in experimental observations), $\Delta W_i > 0$ and oscillations are amplified; i.e., a flutter instability ensues (Benjamin, 1961a, b; Gregory and Païdoussis, 1966a, b; Païdoussis, 1998).

Before considering the outside flow, it is instructive to consider briefly the case of reverse inside flow (the aspirating pipe case). In the simple-minded approach adopted by Païdoussis and Luu (1985), one obtains

$$\Delta W_i = M_f U_i \int_0^T \left[\left(\frac{\partial w}{\partial t} \right)_L^2 - U_i \left(\frac{\partial w}{\partial t} \right)_L \left(\frac{\partial w}{\partial x} \right)_L \right] \mathrm{d}t, \tag{46}$$

and hence the reverse dynamics: the system is unstable by flutter at infinitesimal U_i in the absence of dissipation (which we know is not negligible) and, if dissipation is accounted for, in any case for small U_i; then, at higher U_i, when the second term becomes important, the system regains stability. As discussed in Païdoussis (1999), the main fallacy here is that the intake flow resembles more a sink flow than a reversed jet, and this results in a depressurization *vis-à-vis* the ambient at the intake. As suggested by Kuiper and Metrikine (2005), this depressurization may have been overestimated; therefore, the expression in square brackets in Eq. (46) would have to be modified to $[(\partial w/\partial t)_L^2 - \overline{\alpha} U_i (\partial w/\partial t)_L (\partial w/\partial x)_L]$, with $\overline{\alpha}$ being of the order of $\frac{1}{2}$. Then, Païdoussis et al. (2005) showed that the first term in the expression, related to the Coriolis acceleration, vanishes completely because there is an intake force equal to $-M_f U_i (\partial w/\partial t)$ associated with the change in the lateral momentum of the flow from essentially zero just outside the pipe to $M_f U_i (\partial w/\partial t)$ just inside. This gives rise to a shear force at inlet which eliminates the first term in the square brackets. Also, a slightly more complex interpretation of $\overline{\alpha}$ was provided, suggesting that $0 < \overline{\alpha} < \frac{1}{2}$. The net result is that Eq. (46) is replaced by

$$\Delta W_i = -\overline{\alpha} M_f U_i^2 \int_0^T \left(\frac{\partial w}{\partial t} \right)_L \left(\frac{\partial w}{\partial x} \right)_L \mathrm{d}t. \tag{47}$$

Details are given in Païdoussis et al. (2005). Clearly, if $\overline{\alpha} = 0$ (for maximum intake depressurization), $\Delta W_i = 0$ regardless of the value of U_i. However, for $0 < \overline{\alpha} < \frac{1}{2}$, instability may occur, depending on the magnitudes of $U_i, \overline{\alpha}$ and dissipation.

The purpose of this recourse to the aspirating pipe system is to consider whether the foregoing considerations have any bearing on the reverse outside flow present in the problem at hand.

Based on the work for a cantilevered cylinder in flow directed from the fixed towards the free end, and also for towed cylinders in quiescent fluid, by (i) reversing the flow, (ii) assuming a blunt free end, (iii) assuming the same frictional coefficient c_f in both F_N and F_L as in Eqs. (15), (iv) neglecting dissipation and (v) neglecting any form drag at the upstream end (as the flow does not directly impinge thereon), one can write (Païdoussis, 2004, Sections 8.3.3 and 8.9.6)

$$\Delta W_o = \rho_f A_o U_o \int_0^T \left[\left(\frac{\partial w}{\partial t} \right)_L^2 - U_o \left(\frac{\partial w}{\partial t} \right)_L \left(\frac{\partial w}{\partial x} \right)_L \right] \mathrm{d}t. \tag{48}$$

Clearly, this suggests that, in the absence of dissipation, the effect of the outside flow is to destabilize the system, and that when U_o is high the system would be restabilized.

In terms of the foregoing discussion on the aspirating pipe, let us consider if any modifications or corrections to Eq. (48) are indicated. First, it is noted that the flow in this case is not accelerated axially from essentially zero (or a very small value) to U_o as it enters the annulus; hence, the second term remains unaltered; moreover, the mean pressure changes (the head loss) associated with flow reversal have been taken into account, albeit very approximately. Concerning the first term of Eq. (48), it is true that there is a lateral relative velocity change from zero just upstream to $(\partial w/\partial t)_L$ at the downstream end, but this does not translate to a shear force at $x = L$ associated with this velocity change; the fluid is "free", rather than being "captured" by the pipe at $x = L$. This agrees with the traditional theory of axial flow over a cylinder (Hawthorne, 1961; Païdoussis, 1966, 1973, 2004), finding that, unless there is a tapering end (rather than the cylinder having a square-cut end), no shear force materializes. Nevertheless, there may be a residual effect, such that the first term in Eq. (48) should be replaced by $\alpha(\partial w/\partial t)_L^2$, with $\alpha < 1$. For small U_o, however, this would hardly affect the dynamics qualitatively; it would simply delay the crossing of $\mathscr{I}m(\omega_i)$ from positive to negative to relatively higher values of u_o in Figs. 7, 8 and 10.

7. Conclusions

A theoretical model has been developed for the dynamics of a hanging tubular cantilever, centrally located in a cylindrical container, with fluid flowing inside the cantilever, exiting from the free end, being deflected at the bottom of the container, and thereafter flowing upwards in the annular space between cantilever and container. This configuration was inspired by the geometry of a drill-string with a floating fluid-powered drill-bit at the lower end.

It was found that, if the annular space is wide, the dynamics is dominated by the inside flow (i.e. the flow within the drill string), and the system loses stability by flutter. At low flow velocities, the flow damps the system, further to the damping due to the mere presence of the fluid surrounding the cantilever.

For narrower annuli (such that the ratio of container diameter to cylinder external diameter α_{ch} is 1.2), the dynamics is dominated by the outside (annular) flow. In this case, the flow destabilizes the system, inducing flutter at relatively low flow velocities (just high enough to overcome the effect of the dissipative viscous forces). Thus, for the very slender system considered in the calculations, inspired by the drilling system, if $\alpha_{ch} = 1.2$, the dimensionless inside flow velocity necessary to cause flutter was found to be $u_i = 2.12$, corresponding to a flow velocity of $U_i = 2.44\,\mathrm{m/s}$; for $\alpha_{ch} = 1.1$, $U_i = 1.11\,\mathrm{m/s}$, which is even smaller. However, as discussed in Section 6, the magnitude of the destabilizing force may be overestimated due to end-effects, and the actual critical flow velocities may be somewhat larger. Therefore, comparison with experimental values, when they become available, would be useful.

From the viewpoint of string-drill dynamics this is interesting for the following reason: it shows that, even if the drill-bit never makes mechanical contact with the drill-string, the system is unstable by flutter, whereupon the string would soon touch the surrounding walls and buckle; it has been shown that the critical flow velocity for buckling of a clamped-pinned system is always inferior to that for flutter of the cantilevered one (Païdoussis, 1980, 1998, 2004). Of course, in a real system, effective contact between the drill-bit and the drill-string is inevitable, and so the dynamics is more likely to resemble those of a pipe with clamped or pinned ends (Païdoussis, 1998; Zhang and Miska, 2005); the contact is likely to be intermittent, and hence, because of impacting with the channel and the switching in dynamical state (clamped-free to clamped-pinned and back), complex dynamics would result; cf. Païdoussis et al. (1989).

The most interesting aspect of this work is the finding that such a system becomes unstable by single-degree-of-freedom flutter at very small flow velocities. Thus, at flow velocities close but inferior to the critical, the system would have an arbitrarily small damping, which commends it for MEMS/nanotechnology applications, as mentioned in the Introduction.

Acknowledgements

The authors gratefully acknowledge the support by the Natural Sciences and Engineering Research Council of Canada (NSERC).

References

Bajaj, A.K., Sethna, P.R., 1984. Flow induced bifurcations to three-dimensional oscillatory motions in continuous tubes. SIAM Journal of Applied Mathematics 44, 270–286.

Basak, S., Raman, A., Garimella, S.V., 2006. Hydrodynamic loading of microcantilevers vibrating in viscous fluids. Journal of Applied Physics, 99, #114906.

Batchelor, G.K., 1967. An Introduction to Fluid Dynamics. Cambridge University Press, Cambridge.

Benjamin, T.B., 1961a. Dynamics of a system of articulated pipes conveying fluid. I. Theory. Proceedings of the Royal Society (London) A 261, 457–486.

Benjamin, T.B., 1961b. Dynamics of a system of articulated pipes conveying fluid. II. Experiments. Proceedings of the Royal Society (London) A 261, 487–499.

Berg, R.E., Collier, M.R., 1989. The Feynman inverse sprinkler problem: a demonstration and quantitative analysis. American Journal of Physics 57, 654–657.

Burg, T.P., Manalis, S.R., 2003. Suspended microchannel resonators for biomolecular detection. Applied Physics Letters 83, 2698–2700.

Cesari, F., Curioni, S., 1971. Buckling instability in tubes subject to internal and external axial fluid flow. In: Proceedings of the 4th Conference on Dimensioning. Hungarian Academy of Science, Budapest, pp. 301–311.

Chen, S.S., 1981. Fluid damping for circular cylindrical structures. Nuclear Engineering and Design 63, 81–100.

Chen, S.S., Wambsganss, M.W., Jendrzejczyk, J.A., 1976. Added mass and damping of a vibrating rod in confined viscous fluids. Journal of Applied Mechanics 43, 325–329.

Chung, J.S., Whitney, A.K., Loden, W.A., 1981. Nonlinear transient motion of deep ocean mining pipe. ASME Journal of Energy Resources Technology 103, 2–10.

Creutz, E., 2005. Feynman's reverse sprinkler. American Journal of Physics 73, 198–199.

Deepak, C.R., Shajahan, M.A., Atmanand, M.A., Annamalai, K., Jeyamani, R., Ravindran, M., Schulte, E., Handschuh, R., Panthel, J., Grebe, H., Schwartz, W., 2001. Development tests on the underwater mining system using flexible riser concept. In: Proceedings of the 4th ISOPE Ocean Mining Symposium, Cupertino, CA, USA, pp. 94–98.

Den Hartog, J.P., 1969. John Orr memorial lecture: recent cases of mechanical vibration. The South African Mechanical Engineer 19, 53–68.

Forrester, A.T., 1986. Inverse sprinklers: a lesson in the use of a conservation principle. American Journal of Physics 54, 798–799.

Fukuma, T., Kobayashi, K., Matsushinge, K., Yamada, H., 2005. True atomic resolution in liquid by frequency-modulation force microscopy. Applied Physics Letters 87, 034101-1-3.

Gleick, J., 1992. Genious. Pantheon Books, New York.

Gregory, R.W., Païdoussis, M.P., 1966a. Unstable oscillation of tubular cantilevers conveying fluid. I. Theory. Proceedings of the Royal Society (London) A 293, 512–527.

Gregory, R.W., Païdoussis, M.P., 1966b. Unstable oscillation of tubular cantilevers conveying fluid. II. Experiments. Proceedings of the Royal Society (London) A 293, 528–542.

Grigoriev, J.V., 1978. Stability of a drill tube column with an initial curvature in the axial stream (in Russian). Journal of Bauman Moscow State Technical University: Mashinostronye 5, 23–28.

Hannoyer, M.J., 1972. A solution to linear differential equations in the field of dynamics of continuous systems. Mechanical Engineering Research Laboratories Report MERL-72-5, McGill University. Available from ⟨http://digital.library.mcgill.ca/pse⟩. (Once on the site, select: Mechanical Engineering.)

Hannoyer, M.J., Païdoussis, M.P., 1978. Instabilities of tubular beams simultaneously subjected to internal and external axial flows. ASME Journal of Mechanical Design 100, 328–336.

Hawthorne, W.R., 1961. The early development of the Dracone flexible barge. Proceedings of the Institution of Mechanical Engineers 175, 52–83.

Hsu, L., 1988. Inverse sprinklers: two simple experiments and the resolution of the Feynman–Forrester conflict. American Journal of Physics 56, 307–308.

Idel'chik, I.E., 1986. Handbook of Hydraulic Resistance. Hemisphere, New York.

Kuiper, G.L., Metrikine, V.A., 2005. Dynamic stability of a submerged, free-hanging riser conveying fluid. Journal of Sound and Vibration 280, 1051–1065.

Kuiper, G.L., Metrikine, V.A., 2006. Experimental investigation of dynamic stability of a free hanging pipe conveying fluid. Book of Abstracts, EUROMECH 484, Delft University, pp. 37–38.

Kuiper, G.L., Metrikine, V.A., 2008. Experimental investigation of dynamic stability of a cantilever pipe aspirating fluid. Journal of Fluids and Structures, 24, in press.

Luu, T.P., 1983. On the dynamics of three systems involving tubular beams conveying fluid. M.Eng. Thesis, Department of Mechanical Engineering, McGill University, Montreal, Qué., Canada.

Païdoussis, M.P., 1966. Dynamics of flexible slender cylinders in axial flow. Part 1: theory. Journal of Fluid Mechanics 26, 717–736.

Païdoussis, M.P., 1970. Dynamics of tubular cantilevers conveying fluid. Journal of Mechanical Engineering Science 12, 85–103.

Païdoussis, M.P., 1973. Dynamics of cylindrical structures subjected to axial flow. Journal of Sound and Vibration 29, 365–385.

Païdoussis, M.P., 1980. Flow-induced vibrations in nuclear reactors and heat exchangers: practical experiences and state of the knowledge. In: Naudascher, E., Rockwell, D. (Eds.), Practical Experiences with Flow-Induced Vibrations. Springer, Berlin, pp. 1–81.

Païdoussis, M.P., 1998. Fluid–Structure Interactions: Slender Structures and Axial Flow, vol. 1. Academic Press, London.
Païdoussis, M.P., 1999. Aspirating pipes do not flutter at infinitesimally small flow. Journal of Fluids and Structures 13, 419–425.
Païdoussis, M.P., 2004. Fluid–Structure Interactions: Slender Structures and Axial Flow, vol. 2. Elsevier Academic Press, London.
Païdoussis, M.P., 2005. Some unresolved issues in fluid–structure interactions. Journal of Fluids and Structures 20, 871–890.
Païdoussis, M.P., Besançon, P., 1981. Dynamics of arrays of cylinders with internal and external axial flow. Journal of Sound and Vibration 76, 361–380.
Païdoussis, M.P., Luu, T.P., 1985. Dynamics of a pipe aspirating fluid, such as might be used in ocean mining. ASME Journal of Energy Resources Technology 107, 250–255.
Païdoussis, M.P., Li, G.X., Moon, F.C., 1989. Chaotic oscillations of the autonomous system of a constrained pipe conveying fluid. Journal of Sound and Vibration 135, 1–19.
Païdoussis, M.P., Grinevich, E., Adamovic, D., Semler, C., 2002. Linear and nonlinear dynamics of cantilevered cylinders in axial flow. Part 1: physical dynamics. Journal of Fluids and Structures 16, 691–713.
Païdoussis, M.P., Semler, C., Wadham-Gagnon, M., 2005. A reappraisal of why aspirating pipes do not flutter at infinitesimal flow. Journal of Fluids and Structures 20, 147–156.
Pramila, A., 1992. Undamped cantilever aspirating fluid may be stable. Rakenteiden Mekaniikka 25, 3–14.
Putman, C.A.J., Van der Werf, K.O., De Grooth, B.G., Van Hulst, N.F., Greve, J., 1994. Tapping mode atomic force microscopy in liquid. Applied Physics Letters 64, 2454–2456.
Sinyavskii, V.F., Fedotovskii, V.S., Kukhtin, A.B., 1980. Oscillation of a cylinder in a viscous liquid. Prikladnaya Mekhanika 16, 62–67.
Taylor, G.I., 1952. Analysis of the swimming of long and narrow animals. Proceedings of the Royal Society (London) A 214, 158–183.
Wang, X., Bloom, F., 1999. Dynamics of a submerged and inclined concentric pipe system with internal and external flows. Journal of Fluids and Structures 13, 443–460.
Zhang, Q., Miska, S., 2005. Effects of flow–pipe interaction on drill pipe buckling and dynamics. ASME Journal of Pressure Vessel Technology 127, 129–136.